THE PENNSYLVANIA STATE UNIVERSITY
SCHREYER HONORS COLLEGE

SCHOOL OF SCIENCE, ENGINEERING, AND TECHNOLOGY

SEARCH FOR NEW SOURCES OF VERY-HIGH-ENERGY GAMMA RAYS

KENYA MITCHELL
Spring 2024

A thesis
submitted in partial fulfillment
of the requirements
for baccalaureate degree(s)
in Mathematical Sciences
with honors in Mathematical Sciences

Reviewed and approved* by the following:

Miguel Mostafá
Dean of College of Science and Technology
Affiliate Faculty from Temple University
Thesis Supervisor

Stephane Coutu
Professor of Physics and Astronomy and Astrophysics
Faculty Reader

Gina Brelsford
Director of Capital College Honors
Honors Adviser

* Signatures are on file in the Schreyer Honors College.
NOTE: Signatory Page Template must be completed on special archival paper & turned in as a hardcopy

ABSTRACT

In January of 2021, the HAWC observatory released their third catalogue of very-high-energy gamma ray sources. In this catalogue, 20 of the 65 sources were labeled unassociated. Meaning of all previously discovered sources, they have no high energy counterpart within 1°. From these 20 sources, it was seen that three sources 3HWC J0621+382, 3HWC J0631+107, and 3HWC J1739+099 were closely associated with pulsars PSR J0622+3749, PSR J0631+1036, and PSR J1740+100 respectively. These pulsars are listed in the ANTF pulsar catalog. It is important that these three sources be further studied, as the pulsar association can give clues regarding the origin of gamma ray acceleration. To expand the investigation of these sources, a morphological and spectral analysis was conducted to determine changes in each source's extension and level of emission. Comparisons between pulsar data and HAWC data were also conducted to verify that each experiment was seeing the same thing. Multiple software packages were utilized to visualize the data. The Multi-Mission Maximum Likelihood framework (3ML) in conjunction with the HAWC accelerated likelihood (HAL) plugin is used to fit source spectrums and determine morphology. After analyzing data from HAWC's datasets of 1,523 days and 2,770 days, it was concluded that each source exhibited significant growth in intensity over time. Future work will include a multi-wavelength analysis using data from other gamma-ray experiments.

TABLE OF CONTENTS

LIST OF FIGURES

LIST OF TABLES

ACKNOWLEDGEMENTS

I would like to start by thanking my thesis supervisor, Dr. Miguel Mostafá, for the immense amount of encouragement and support he has provided for the duration of this project. I also would like to thank Dr. Hugo Ayala Solares for answering my many, many questions and providing me with many resources for my research. Next, I would like to thank Dr. Gina Brelsford for also being a source of encouragement during this process. Being able to share my struggles and doubts in HONOR 401 was cathartic during a stressful time. Lastly, I would like to thank my parents for giving me the foundation to not only be a successful honors student, but a functioning and contributing member of society. Being able to make them proud makes all the long nights worth it.

Chapter 1: Introduction

Very-High-Energy (VHE) gamma rays are the basis of many open questions of astrophysics. As they originate from the most extreme environments in the universe, studying these electromagnetic waves can yield information about the nature of both astrophysical objects, such as black holes and neutron stars, and extreme particle acceleration which leads us to learn more about the origins of cosmic rays. Due to this overarching importance to many aspects of space exploration, it is important that new sources of VHE gamma rays are discovered.

Present day research into VHE gamma rays fits into an area of science known as particle physics. This is due to the way gamma rays interact with matter. When a gamma ray enters Earth's atmosphere, it creates an electromagnetic cascade – a particle shower in other words. The direction and energy level of these particles can then be studied through ground-based detection. Ground-based observatories spend years collecting data on these particle showers until sources of gamma-ray energy can be identified within statistical certainties. This thesis will analyze three such sources to determine their consistency over time, according to standard expectation in ground-based gamma-ray astronomy. There will also be an analysis of spectral and morphological properties to further characterize the types of sources they are.

Chapter 2: Literature Review

2.1. Cosmic Rays

Cosmic rays are high-energy particles that travel across space at close to light-speed. These particles enter Earth’s atmosphere every day at a rate of about 1,000 particles per square meter per second. Most cosmic rays are atomic nuclei consisting of many elements found in the periodic table. Their make-up varies with the energy levels of the particles; with 90% being protons, 9% being alpha particles (helium) and 1% being heavier elements (Resconi et al., 2016).

Despite being discovered in 1912 by Victor Hess, it was not until the 1930’s that these particles’ truly enigmatic nature was realized. Cosmic rays are electrically charged, causing them to be affected by magnetic fields. Passing through a magnetic field causes the path of cosmic ray particles to become deflected or randomized. Consequently, their arrival direction at Earth becomes randomized also, causing the origin of the particles’ acceleration to become untraceable (Richard Mewaldt, 2009). It is only at the ultra-high-energy (UHE) regime that this can be overcome (Pierre Auger Collaboration et al., 2022).

There are still ways to figure out the places of cosmic-ray production without detecting them directly. Interactions of high-energy cosmic rays with interstellar gas and radiation fields can lead to the creation of gamma rays – high-energy particles that travel in a straight line from their source to Earth’s surface (Funk, 2015). We can take advantage of this to discover the sources of cosmic rays.

2.2. Gamma Rays

Gamma rays are the highest frequency radiation found in the electromagnetic spectrum. They travel to Earth in a straight-line due to their inability to be accelerated. So, any known acceleration and charge comes from the associated cosmic rays. Upon reaching their destination, gamma rays interact with Earth's atmosphere, and therefore, we observe them either directly above the atmosphere or indirectly detecting the particles and radiation that result from these interactions. For example, the gamma-ray sky can be seen through dedicated satellites like the Compton Observatory. Unlike other members of the electromagnetic spectrum like x-rays and visible light, gamma rays cannot be reflected through mirrors. Gamma-ray telescopes instead utilize Compton scattering to capture the rays. This is an interaction between an electron and high-energy photon (i.e., a gamma ray), where the energy of the electron is partially transferred to the photon. This transfer causes the photon to deflect from its original course, and "scattering" elsewhere (White & Pharoah, 2014). An example of this is found in the Fermi Large Area Telescope (Fermi-LAT). A space-based detector that studies gamma-rays in the range of 2×10^5 electron-Volts (eV) to 300×10^9 eV. A documented pitfall to Compton Scattering as a detection method, is the direct correlation between gamma-ray energies and the area needed to collect the events through telescope. Once energies cross 10^{12} eV, the size of the telescopes needed to study these events is too large and is no longer practical to launch into space (De Angelis & Mallamaci, 2018). As mentioned before, high-energy gamma rays are studied through indirect methods. When high-energy gamma rays enter Earth's atmosphere, they collide with initial surrounding particles and produce secondary particles. These secondary particles then collide with other particles, creating a cascading “particle shower.” These particles showers are how gamma rays are then studied to determine the location of their sources.

2.3. Very High Energy (VHE) Gamma Rays

Gamma rays span an energy range of 10^5 eV to over 10^{15} eV. Above the threshold of around 10^{11} eV they are classified as Very-High-Energy (VHE) gamma rays (Veritas, 2010). Apart from their association with the sources of cosmic rays, gamma rays provide important information about astrophysical objects. VHE gamma rays are born in some of the most extreme environments in the universe. Possible sources of VHE gamma rays include supernova remnants, active galactic nuclei, and pulsars. We observe VHE gamma rays indirectly using ground-based telescopes or arrays of particle detectors (Bose & Chitnis, 2022).

2.4. Detection of VHE Gamma Rays

A specific example of a ground-based VHE gamma-ray detector is the High-Altitude Water Cherenkov (HAWC) observatory is located on the flanks of the Sierra Negra volcano near Puebla, Mexico at an altitude of 4100 meters (13,500 feet). Having been completed in 2015, HAWC is known for its large field of view and sensitivity to the highest energies of gamma rays. HAWC’s instantaneous field-of-view allows observations at declinations between -26° and 64°, i.e., two-thirds of the sky every day. HAWC detects gamma rays with energies in the range of 1 to 300 Tera-electron Volts (TeV) through an array of 300 water Cherenkov detectors (Abeysekara et al., 2023). Each water Cherenkov detector is a 200,000-liter tank of water that has been fitted with four photomultiplier tubes (PMTs). This is to utilize the Cherenkov effect (Malone, 2018), which occurs when a charged particle passes through the purified water in the tanks faster than the speed of light, and consequently emits ultraviolet radiation. This light produces photoelectrons in the PMTs, allowing particle showers to be reconstructed and further studied (Albert et al., 2020). Reconstruction is necessary to determine the arrival direction and size of the shower. The size then can be used as an approximation for the shower energy (Abeysekara et al., 2017).

2.5. Sources of VHE Gamma Rays

As was previously mentioned, gamma rays are emitted from some of the most extreme environments in the galaxy. Although there are several known sources, some of the more commonly observed are supernova remnants (SNRs) and pulsars. SNRs are the remains of powerful and bright explosion of a star. When a supernova explosion occurs, the huge amount of resultant energy interacts with nearby molecular clouds and accelerates cosmic rays. One of the most well-known examples of this kind of interaction within our galaxy is IC 443, an SNR first observed in VHE by the Fermi-LAT satellite experiment. This source is one of the highest-energy sources currently recorded by the observatory and is estimated to be around 10,000 years old (Ackermann et al., 2013).

Pulsars are high-energy, rotating neutron stars. They can emit pulsed energy ranging from radio waves up to gamma rays in the VHE range. They are formed from the core of a massive star that has collapsed under the weight of its own gravity. The momentum from this results in the pulsar spinning at a rate of many revolutions per second. The majority of today’s known gamma-ray pulsars have been recorded by the

Fermi-LAT as well (Grenier & Harding, 2015).

Chapter 3: Sources of Interest

HAWC's most recent catalog of sources, the 3HWC Catalog, was published in 2019. Within this catalog, there are 65 recorded sources, studied over 1523 days. Of these 65 sources, 20 are labeled as "unassociated" or "orphan" sources. This labeling describes the sources' location being more than one degree in separation away from any other previously recorded source (Albert et al., 2020). This is important because it means that HAWC is seeing sources in new regions of space. To be included in the catalog, each source's local maxima had to hold a statistical significance greater than 5 standard deviations from a random background fluctuation.

A similar study, combined with restructured criteria for source promotion was conducted for the unassociated sources seen in 3HWC. Both morphological and spectral analyses were necessary to determine changes in each source's extension and level of emission. The analyses were conducted using a framework for multi-wavelength data analysis called the Multi-Mission Likelihood framework (3ML). In particular, the HAWC Accelerated Likelihood (HAL) plugin is used to handle HAWC data. Maximum likelihood estimation is a well-known statistical inference method that when given a set of measurements, interprets physical parameters of an assumed probability distribution by maximizing the value of a likelihood function. This allows for the optimization of the spectrum and morphology of a source, which in turn allows detection of source significance by calculating a test statistic (TS), where $TS = -2\log\left(\frac{\mathcal{L}_0}{\mathcal{L}}\right)$, with $\mathcal{L}_0$ and $\mathcal{L}$ being maximum likelihood values (Albert et al., 2020).

The two probability distributions applied to the HAWC sources were a simple power-law of the form $\frac{dN}{dE} = N_0(\frac{E}{E_0})^{-\gamma}$ and log-parabola denoted $\frac{dN}{dE} = N_0(\frac{E}{E_0})^{-\alpha-\beta\ln(\frac{E}{E_0})}$. Where N_0 is the source's normalization value, E_0 is the pivot energy, and γ is the index. The equation for the log-parabola has the added fit parameters α and β. The sources were fitted to these distributions with either a point-source or extended-source model. Simply put, an extended source is a source that covers a large region of the sky, while a point source is one that doesn't. It is important to note that the power law and log parabola are what are known as nested models. A nested model uses the same parameters as another model but includes at least one additional value to be estimated. In this case, the power law is the reduced model, as it can obtained by setting the β value in the log parabola function to zero. When any source is fitted to both these models, a maximum likelihood ratio test can be performed to determine the more favorable fit.

A maximum likelihood ratio test estimates a p-value that can be used in a statistical hypothesis test. More specifically, a chi-square test was used to determine the plausibility of each hypothesis. To conduct this test, the maximum likelihood values of each comparable fit were plugged into a chi-square test statistic, denoted $TS_{chi} = -2(\log(likelihood_{full}) - \log(likelihood_{reduced}))$. This value follows a chi-square distribution with n degrees of freedom, where n equals the difference in degrees of freedom between the two nested models. Note that for the power law and log parabola models, $n = 1$. Once the p-value is estimated from this distribution, a null hypothesis, H_0, can be accepted or rejected in favor of an alternate hypothesis, H_1. Here, H_0 states that there is no statistically significant difference between how well each model fits a source, while H_1 says the full model is the better fit. This choice is made based on a 95% confidence level. So, if the p-value is smaller than 0.05, the null hypothesis is rejected, if the p-value is greater than or equal to 0.05, the null hypothesis is accepted.

For each model, 3ML calculates a value known as the Akaike Information Criterion (AIC, Albert et al., 2020), denoted $AIC = 2k - 2\ln(\mathcal{L})$, where k is the number of parameters being fitted and $\mathcal{L}$ is the maximum likelihood. When comparing fits of non-nested models, the one with the smallest AIC is considered better. Here, non-nested refers to models of the same distribution, but different morphologies.

Table 1. Twenty Unassociated sources from the 3HWC catalog.

HAWC	l [°]	b [°]	4FGL (°)	Class	ATNF (°)	SNRCat (°)	SNR Type
3HWC J0621+382	175.44	10.97	4FGL J0620.3+3804 (0.22)	bcu	J0622+3749 (0.42)	...	...
3HWC J0630+186	193.98	4.02	...	...	J0630+19 (0.94)	...	
3HWC J0631+107	201.08	0.43	4FGL J0631.5+1036 (0.15)	PSR	J0631+1036 (0.14)	...	...
3HWC J0633+191	193.92	4.85	...	...	...	...	...
3HWC J1739+099	33.89	20.34	4FGL J1740.5+1005 (0.22)	PSR	J1740+1000 (0.13)	G034.0+20.3 (0.13)	filled-centre
3HWC J1743+149	39.13	21.68	...	...	...	...	
3HWC J1844−001	31.95	1.50	4FGL J1848.2−0016 (0.99)	...	J1843−0000 (0.27)	...	...
3HWC J1857+051	38.22	1.06	4FGL J1855.2+0456 (0.56)	...	J1857+0526 (0.24)	...	...
3HWC J1915+164	50.19	2.35	4FGL J1912.0+1612 (0.74)	bcu	B1913+16 (0.32)	...	...
3HWC J1918+159	50.16	1.33	...	...	J1918+1541 (0.26)	...	...
3HWC J1923+169	51.58	0.89	4FGL J1925.1+1707 (0.50)	unk	B1921+17 (0.14)	...	...
3HWC J1935+213	56.90	0.39	4FGL J1935.2+2029 (0.89)	PSR	J1936+21 (0.24)	G057.2+00.8 (0.59)	shell
3HWC J1936+223	57.76	0.73	4FGL J1932.2+2221 (0.94)	PSR	J1938+2213 (0.44)	G057.2+00.8 (0.47)	shell
3HWC J1937+193	55.29	−0.98	4FGL J1936.6+1921 (0.21)	...	J1936+20 (0.77)	...	...
3HWC J1951+266	63.23	−0.13	4FGL J1951.6+2621 (0.25)	...	J1952+2630 (0.24)	...	...
3HWC J2005+311	68.74	−0.40	4FGL J2006.2+3102 (0.15)	PSR	J2006+3102 (0.15)	G068.6−01.2 (0.81)	unknown
3HWC J2010+345	72.14	0.56	...	...	...	...	...
3HWC J2022+431	80.52	3.54	...	...	...	...	...
3HWC J2023+324	71.85	−2.77	4FGL J2024.0+3202 (0.43)	unk	...	...	...
3HWC J2043+443	83.74	1.10	4FGL J2047.5+4356 (0.79)	...	...	...	...

Each column of the table lists the following: the names of the sources; the Galactic latitude and Galactic longitude of the sources in degrees; the nearest GeV source found in the 4FGL catalog (Abdollahi et al., 2020); the nearest pulsar; the corresponding separation found in the ANTF catalog (Manchester et al, 2005); the nearest SNR, along with the separation distance and type from the SNR Catalog (Ferrand & Safi-Harb, 2012). Here, PSR refers to a pulsar source and bcu to a blazar candidate of unknown type. From Albert, A., Alfaro, R., Alvarez, C., Camacho, J. A., Arteaga-Velázquez, J. C., Arunbabu, K. P., Rojas, D. A., Solares, H. A., Baghmanyan, V., & Belmont-Moreno, E. (pg. 14) (2020). 3HWC: The third HAWC catalog of very-high-energy gamma-ray sources. *The Astrophysical Journal*, *905*(1), 76.

One of the first goals of this project was to create significance maps for each of these sources listed above using the most recent event reconstruction (internally called Pass 5). A source of interest would be determined by an increase in significance between HAWC's previous dataset (Pass 4) and Pass 5, covering 2770 days of data. Furthermore, if the excess was due to a source of gamma rays, the increase in significance should be proportional to the square root of the additional amount of time in the new dataset. While going through this process, it was discovered that three of the unassociated sources not only had a large increase in significance, but they also were in very close proximity to known pulsars observed by Fermi-LAT, hinting that these pulsars could be related to the acceleration of the newly discovered VHE gamma rays. These three sources are 3HWC J0621+382, 3HWC J0631+107 and 3HWC J1739+099.

To assess the intensity of a source over time, a visualization tool called a significance map is employed. Significance maps are graphical representations of the statistical significance of an event. Significance is measured as the square root of the TS. The higher the $\sqrt{TS}$, the brighter the colors in the map.

Figure 1. Significance maps of 3HWC J0621+382

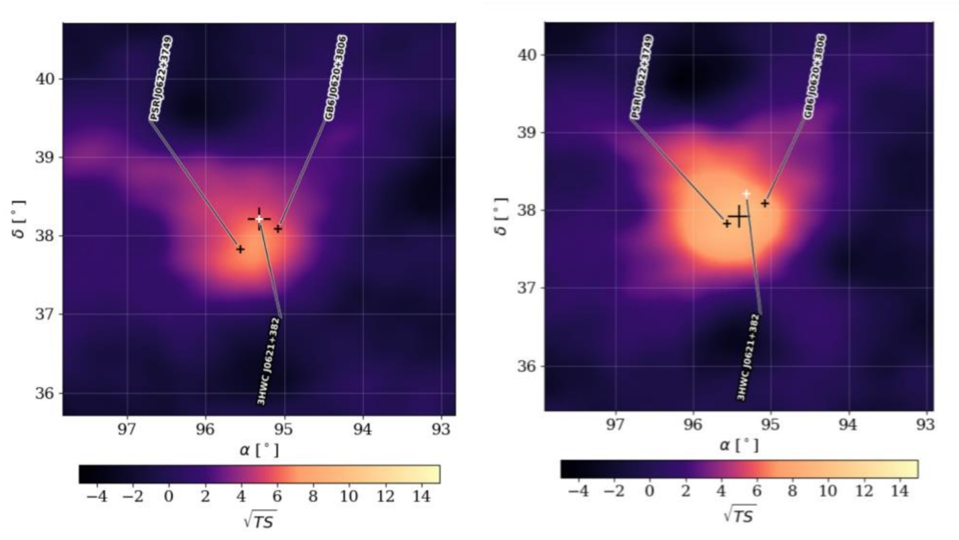

The vertical and horizontal axis give declination and right ascension of the source; the scale along the bottom gives the color corresponding to the $\sqrt{TS}$. The significance map on the left depicts the source using Pass 4 data (1523 days of data). The parameters are taken from the 3HWC catalog. The map on the right depicts the source using Pass 5 data (2770 days of data).

Table 2. Pass 4 and Pass 5 data for 3HWC J0621+382 corresponding to the significance maps.

	Pass 4	**Pass 5**
Radius (°)	0.5	0.5
$\sqrt{TS}$	5.29	8.03
RA (°)	95.32	95.66 ± 0.023
DEC (°)	38.21	38.16 ± 0.009

The table lists the following: radius (the size of the source extension); the $\sqrt{TS}$; the right ascension and declination of the actual source in Pass4 and then the of the max TS in pass5.

As mentioned before, each of the sources studied are closely associated with known pulsars observed by Fermi-LAT in each region. To better determine the pulsars' role in the origin of these newly discovered sources, it is necessary to compare the pulsar data to the data provided by HAWC. This is done by combining data points plotted on a spectral energy distribution (SED). An SED plots a source's flux versus energy. In experiments that use particle arrays rather than telescopes, an SED may plot particle flux versus energy instead. Particle flux is a weighted flux, denoted "E^2 Flux" that makes it easier to see features like cutoffs or a change from one spectral index to another. Figure 2 presents an SED for the pulsar PSR J0622+3749 published by the Large High Altitude Air Shower Observatory (LHASSO). This pulsar was seen in the same region as 3HWC J0621+382 and so the data points presented will be compared to the data points in an SED created using HAWC data.

Figure 2. SED of PSR J0622+3749 presented by LHASSO.

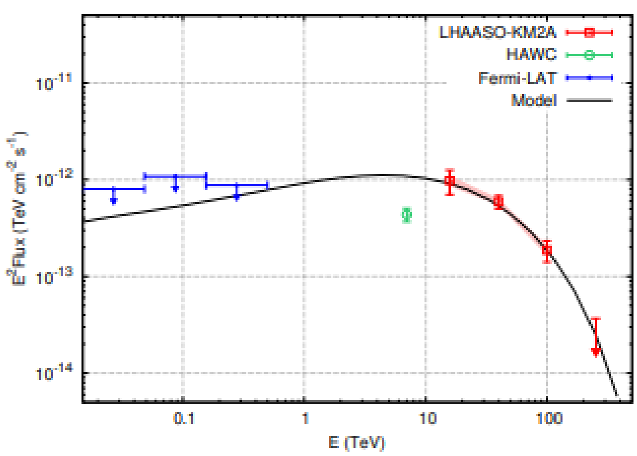

This model is combined with data the HAWC measurement for J0621+382 and upper limits for the pulsar from Fermi-LAT. SED fitted to a pulsar halo model. Aharonian F et al.; LHAASO Collaboration. Extended

Very-High-Energy Gamma-Ray Emission Surrounding PSR J0622+3749 Observed by LHAASO-KM2A. Phys Rev Lett. 2021 Jun 18;126(24):241103. doi: 10.1103/PhysRevLett.126.241103. PMID: 34213924. (Figure 3)

Table 3. Data for PSR J0622+3749 from the Australia Telescope National Facility (ANTF) Pulsar Catalogue.

Ė (EDOT) $[\times 10^{35} \mathrm{erg s}^{-1}]$	$2.7e+34$
Age (kyr)	$2.08e+05$
Distance (kpc)	-
RA (°)	95.5417
DEC (°)	37.8203

The table lists the spin-down energy (EDOT), age of the pulsar in thousands of years, and the distance of the pulsar from Earth, if given.

Figure 3. Significance maps of 3HWC J0631+107.

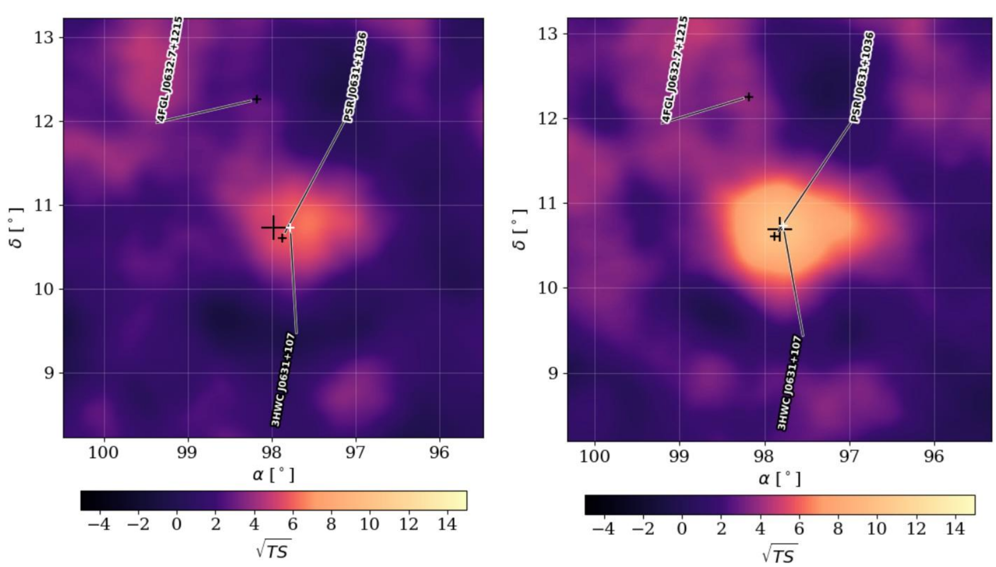

Table 4. Pass 4 and Pass 5 data for 3HWC J0631+107 corresponding to the significance maps.

	Pass 4	**Pass 5**
Radius (°)	0.5	0.5
$\sqrt{TS}$	5.15	6.10
RA (°)	97.98	97.82
DEC (°)	10.73	10.69

Figure 4. SED of PSR J0631+1036 presented by the Magic Atmospheric Gamma Imaging Cherenkov (MAGIC) Telescopes.

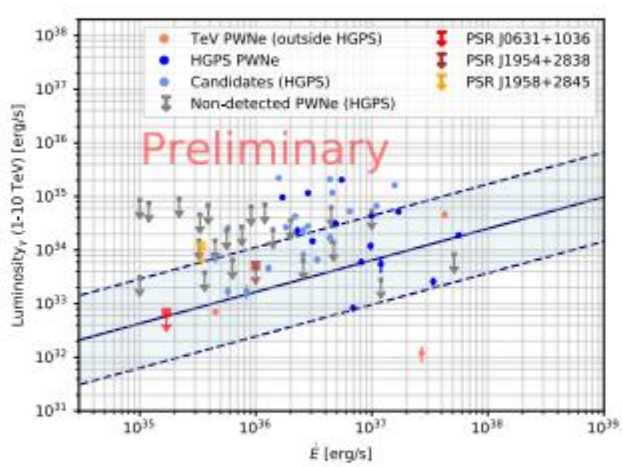

This pulsar was seen in the same region as 3HWC J0631+107. The data is presented as TeV luminosity vs. the characteristic age. The model the data has been fitted to is represented by the blue bands. Fernández Barral, Alba & Blanch Bigas, Oscar & Chatterjee, Anshu & Wilhelmi, E. & Fidalgo, D. & Collaboration, for. (2017). MAGIC observations on Pulsar Wind Nebulae around high spin-down power Fermi-LAT pulsars.

Table 5. Data for PSR J0622+3749 from the Australia Telescope National Facility (ANTF) Pulsar Catalogue.

$\dot{E}$ $[\times 10^{35} \mathrm{ergs}^{-1}]$	1.7e+35
Age (kyr)	43.6
Distance (kpc)	2.10
RA (°)	97.8625
DEC (°)	10.6172

Figure 5. Significance maps of J1739+099.

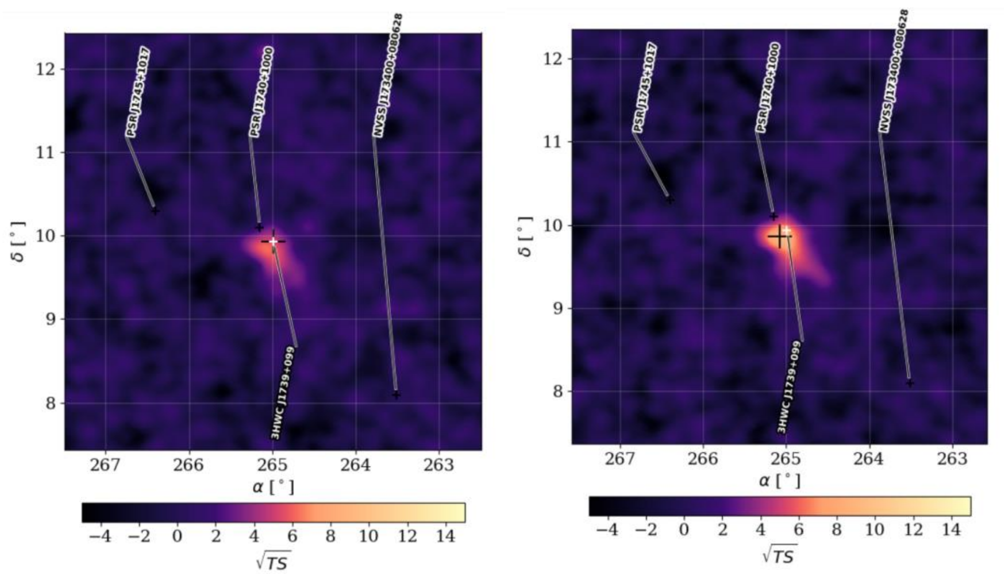

Table 6. Pass 4 and Pass 5 data for 3HWC J1739+099 corresponding to the significance maps.

	Pass 4	**Pass 5**
Radius (°)	0.0	0.0
$\sqrt{TS}$	5.31	7.53
RA (°)	264.99	$265 - 0.00030 + 0.00021$
DEC (°)	9.93	$9.861 - 0.024 + 0.030$

Figure 6. SED of PSR J1740+1000 presented by X-ray Multi-Mirror Mission (XMM-Newton) mission.

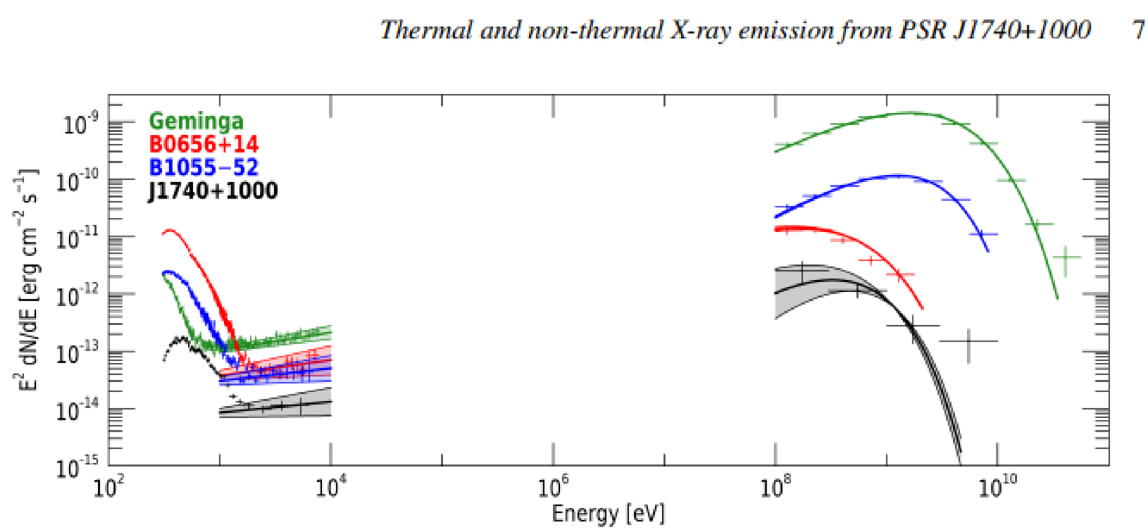

This pulsar was seen in the same region as 3HWC J1739+099. The fit compares the J1740+1000 data to other pulsars that are considered similar. Rigoselli, M., Mereghetti, S., Anzuinelli, S., Keith, M., Taverna, R., Turolla, R., & Zane, S. (2022). Thermal and non-thermal X-ray emission from the rotation-powered radio/γ-ray pulsar PSR J1740+ 1000. *Monthly Notices of the Royal Astronomical Society*, *513*(3), 3113-3121.

Table 7. Data for PSR J1740+1000 from the Australia Telescope National Facility (ANTF) Pulsar Catalogue.

$\dot{E}$ $[\times 10^{35} \mathrm{ergs}^{-1}]$	$2.3e + 35$
Age (kyr)	$1.14e + 05$
Distance (kpc)	1.227
RA (°)	265.1042
DEC (°)	10.0017

Chapter 4: Results

The Crab Nebula is known as a standard reference source in ground-based gamma-ray astronomy. This is due to it being a consistently bright high-energy source for multiple energy bands. This makes it possible to use the Crab as a reference of measurement for other sources. Below is a time vs. significance plot, comparing the Crab and the three HAWC sources to an expected growth trajectory over 2500 days. If a source is steady, the significance of the source will grow with time, like the Crab. This expectation of growth is depicted by the dotted red "expectation" line. This line is calculated by $\sqrt{\frac{t}{500}}$, where t is the number of days observed. The relation with the days observed is estimated from how significance is calculated in a background dominated experiment. Combined with the data points from the three sources, it becomes a plotted visualization of the growth shown in the significance maps. The three HAWC sources have not only grown in intensity over time but have plotted a path like that of the Crab and expected growth. This is evidence that they are behaving as steady sources over an extended period.

Figure 7. Normalized significance vs. time plot for the HAWC sources vs. the Crab Nebula.

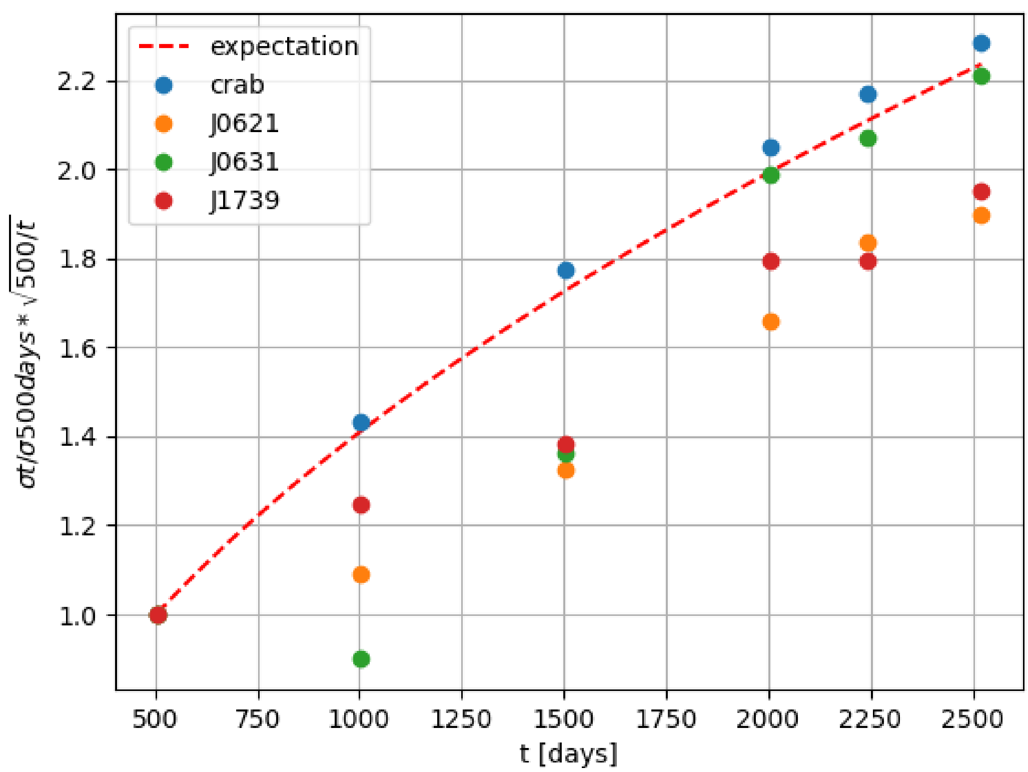

4.1. J0621+382

Figure 8. Extended Gaussian power law model fitted for 3HWC J0621+382.

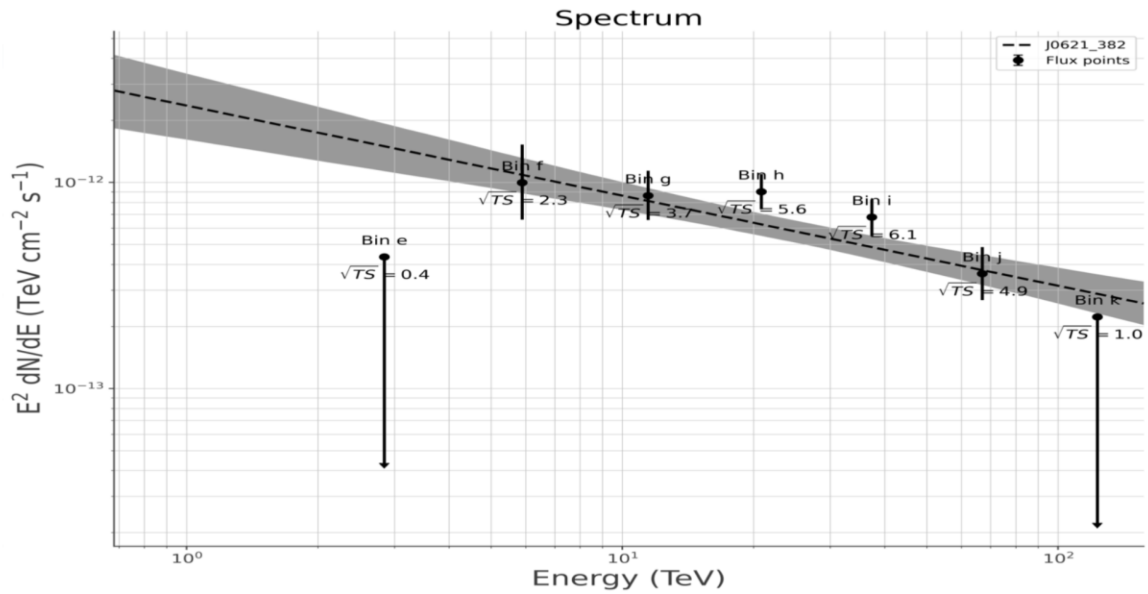

$$\frac{\boldsymbol{dN}}{\boldsymbol{dE}} = (7.3\ \times 10^{-24})(\frac{E}{19.7Tev})^{-2.41}$$

Table 8. Results of J0621+382 power law fit.

RA	95.68 ± 0.01
DEC	38.13 ± 0.01
Extension	$0.54\ \pm 0.6$
Normalization	$(7.3 - 1.1 + 1.2)\ \times\ 10^{-24}$
Index	$-2.41\ \pm 0.08$
Log(Likelihood)	556816
AIC	1113643
BIC	1113707
TS	95

It lists the estimated Right Ascencion and Declination, normalization, extension, index, likelihood result of the fit, AIC and BIC values.

Figure 9. Extended Gaussian log parabola model fitted for 3HWC J0621+382.

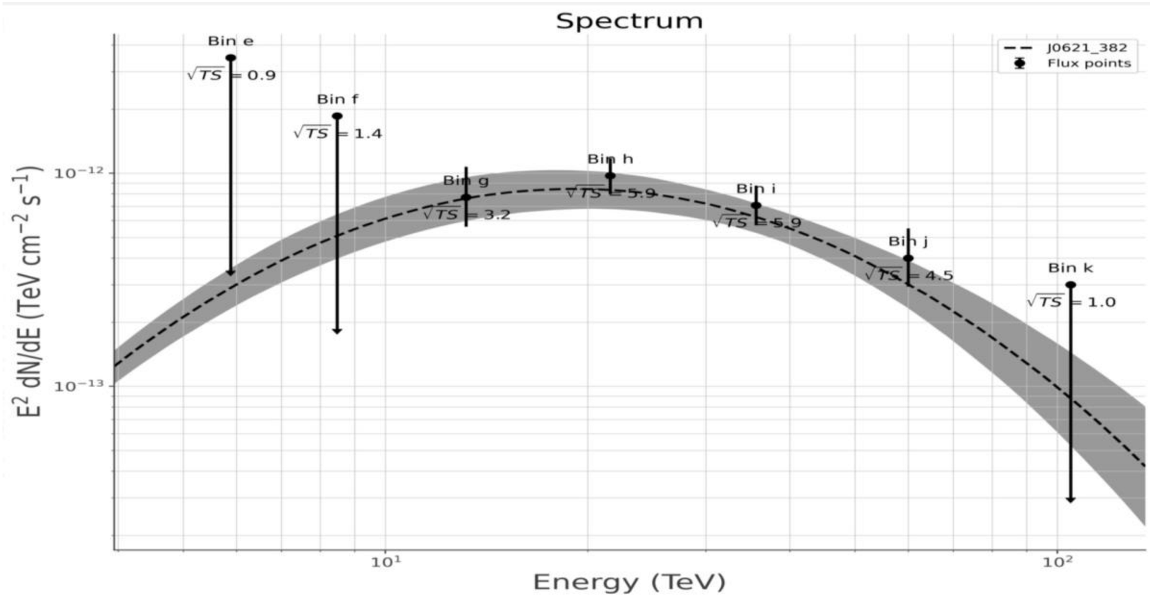

$$\frac{\boldsymbol{dN}}{\boldsymbol{dE}} = (8.1\ \times 10^{-24})(\frac{E}{20Tev})^{1.27-\left(0.65\ln\left(\frac{E}{20Tev}\right)\right)}$$

Table 9. Results of J0621+382 log parabola fit.

RA	95.64 ± 0.01
DEC	38.10 ± 0.01
Extension	$0.54\ \pm 0.6$
Normalization	$(8.1 - 2.1 + 2.5)\ \times\ 10^{-24}$
Alpha	$1.27 - 0.5 + 0.27$
Beta	$0.65 - 0.24 + 0.21$
Log(Likelihood)	186581
AIC	373175
BIC	373252
TS	36

A maximum likelihood ratio was applied to analyze the accuracy of the models fitted to 3HWC J0621+382. The X^2 test statistic was calculate as $TS_{chi} = -2(186581 - 556816) =\ 740470$. This yielded a p-value of 0.00 ... < 0.05 implying that the null hypothesis is to be rejected. Thus, the gaussian log parabola is the more accurate fit for this source. As both fits calculated a gaussian extension of 0.54 degrees, this is the current best fit for that parameter.

4.2. J0631+107

Figure 10. Extended Gaussian power law model fitted for 3HWC J0631+107.

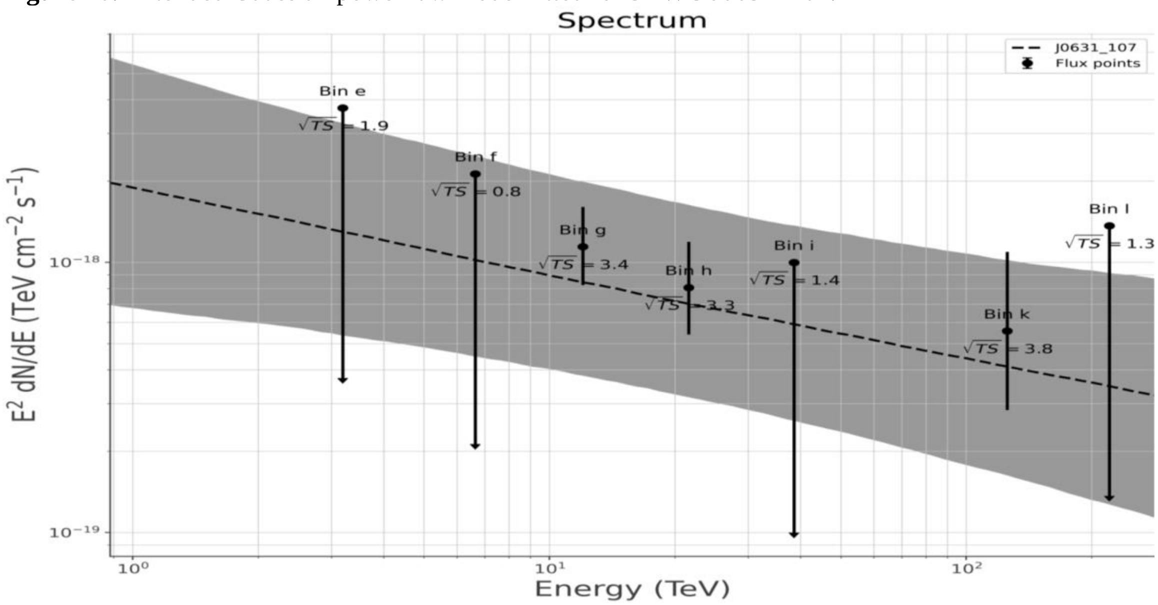

$$\frac{\boldsymbol{dN}}{\boldsymbol{dE}} = (0.18 \times 10^{-29})(\frac{E}{20Tev})^{-2.32}$$

Table 10. Results of J0631+107 gaussian power law fit.

RA	97.782 ± 0.001
DEC	10.690 ± 0.001
Extension	1.1 ± 1.9
Normalization	$(0.18 - 0.18 + 5) \times 10^{-29}$
Index	-2.32 ± 0.21
Likelihood	152300
AIC	304610
BIC	304674
TS	40

Figure 11. Extended disk power law model fitted to 3HWC J0631+107.

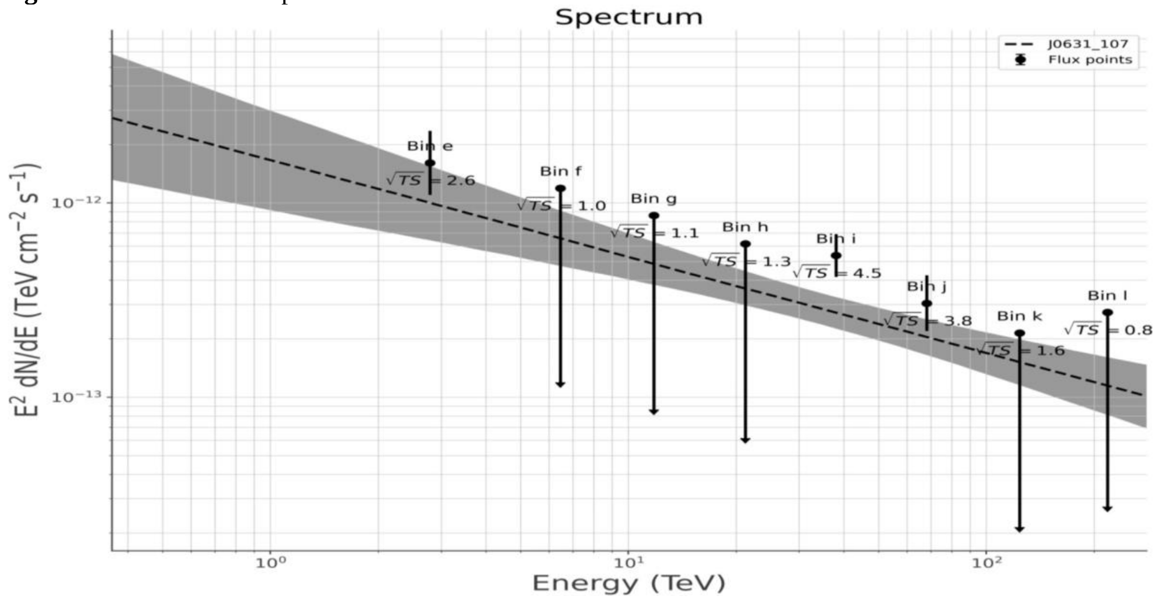

$$\frac{\boldsymbol{dN}}{\boldsymbol{dE}} = (8.3\ \times 10^{-25})(\frac{E}{20Tev})^{-2.38}$$

Table 11. Results of J0631+107 disk power law fit.

RA	97.034 ± 0.0018
DEC	$10.007\ \pm 0.0014$
Extension	$1.10\ \pm 0.15$
Normalization	$(8.3 - 1.3 + 1.5) \times 10^{-25}$
Index	$-2.38\ \pm 0.15$
Likelihood	152842
AIC	305690
BIC	305729
TS	20

The source 3HWC J0631+107 was fitted to a gaussian power law and a disk power law. As the difference between these models is the morphology, they are not considered nested. A comparison of the AIC values for each fit was used to determine the more accurate model. The calculated values are $AIC_{gaussian} =\ 304610$ and $AIC_{disk} =\ 305690$. As $AIC_{gaussian} <\ AIC_{disk}$, the power law gaussian fit is the better fit for this source. This also implies that the favored extension of the source is a disk of 1.10 degrees.

4.3. J1739+099

Figure 12. Point source gaussian power law fitted for 3HWC J1739+099.

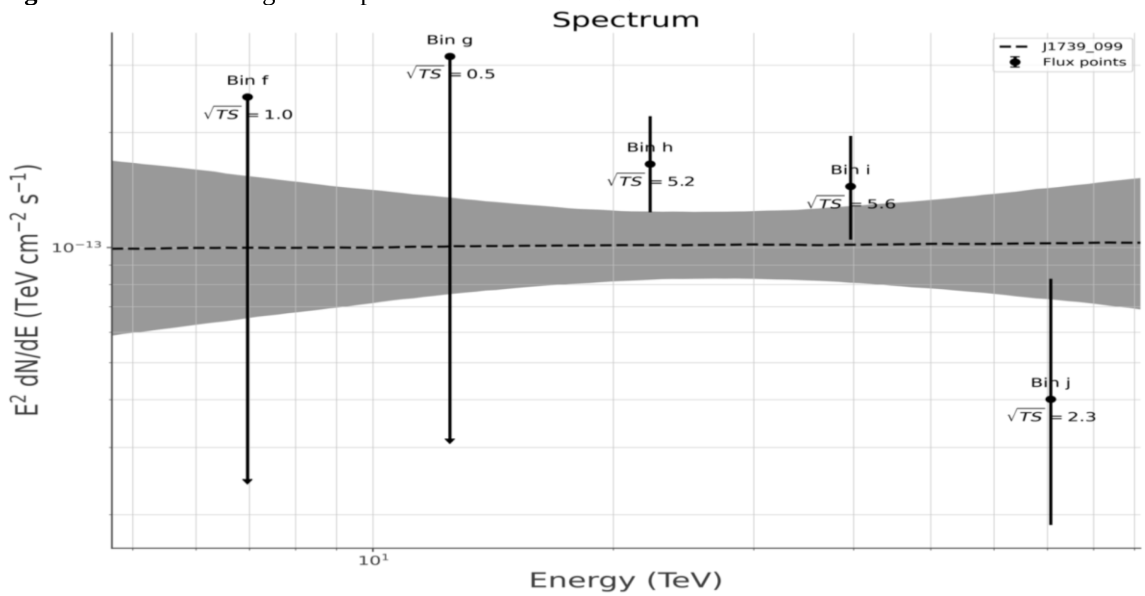

$$\frac{\boldsymbol{dN}}{\boldsymbol{dE}} = (1.01\ \times 10^{-24})(\frac{E}{10Tev})^{-1.99}$$

Table 12. Results of J1739+099 power law fit.

RA	$265.058 \pm\ 0.00021$
DEC	$9.861\ \pm\ 0.025$
Normalization	$(1.01\ -0.28\ +0.4)\ \times\ 10^{-24}$
Index	$-1.99\ \pm 0.27$
Likelihood	37636
AIC	75281
BIC	75328
TS	56

Figure 13. Point source gaussian log parabola fitted to 3HWC J1739+099.

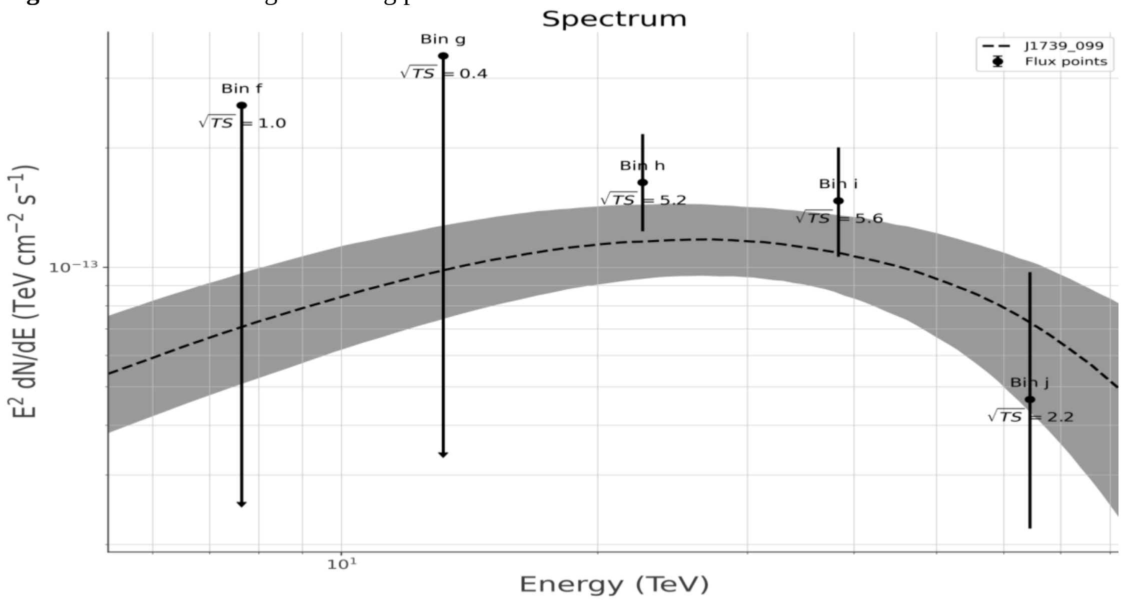

$$\frac{\boldsymbol{dN}}{\boldsymbol{dE}} = (1.2\ \times 10^{-24})(\frac{E}{10Tev})^{-2.63-(0.1\ln\left(\frac{E}{10TeV}\right))}$$

Table 13. Results of J1739+099 log parabola fit.

RA	$265.058\ \pm\ 0.01$
DEC	$9.861 - 0.02 + 0.03$
Normalization	$(1.2\ - 0.4\ + 0.6)\ \times\ 10^{-24}$
Alpha	$2.63 - 2.37 + 1.63$
Beta	$0.1 - 0.9 + 1.9$
Likelihood	37519
AIC	75045
BIC	75081
TS	56

A maximum likelihood ratio was applied to analyze the accuracy of the models fitted to 3HWC J1739+099. The X^2 test statistic was calculate as $TS_{chi} = -2(37519 - 37636) =\ 234$. This yielded a p-value of $0.00 \ldots 7 < 0.05$ implying that the null hypothesis is to be rejected. Thus, the gaussian log parabola is the more accurate fit for this source.

4.4 Future Work

As mentioned before, several other experiments have released pulsar data in the same regions as the 3HWC sources. Further work would include a multi-wavelength analysis of this data to see if these experiments are seeing similar things to HAWC at different energy levels. The experiments in question are LHASSO (PSR J0622+3749), MAGIC (PSR J0631+1036), and XMM-NEWTON (PSR J1740+1000). Each of these observatories detect sources in the ~200 GeV to 1 PeV range, 50 GeV to 30 Tev range, and 0.1 to 15 keV range, respectively. These detection levels span from well-below to slightly above HAWC's 1 to 300 TeV. To conduct this analysis, data from each of the experiments would be combined with HAWC data from their respective regions. This would result in fits to which further spectral and morphological analyses could be applied.

References

Abdollahi, T. F.-L. (2020). Fermi Large Area Telescope Fourth Source Catalog. The Astrophysical Journal Supplement Series, 247(1), 33. https://doi.org/10.3847/1538-4365/ab6bcb

Albert, A., Alfaro, R., Alvarez, C., Camacho, J. A., Arteaga-Velázquez, J. C., Arunbabu, K. P., Rojas, D. A., Solares, H. A., Baghmanyan, V., & Belmont-Moreno, E. (2020). 3HWC: The third HAWC catalog of very-high-energy gamma-ray sources. *The Astrophysical Journal*, *905*(1), 76.

Albert, A., Alfaro, R., Alvarez, C., Camacho, J. R. A., Araya, M., Arteaga-Velázquez, J. C., Arunbabu, K. P., Rojas, D. A., Solares, H. A. A., Baghmanyan, V., Belmont-Moreno, E., Brisbois, C., Caballero-Mora, K. S., Carramiñana, A., Casanova, S., Cotti, U., De la Fuente, E., de León, C., Hernandez, R. D., … Zhou, H. (2020). HAWC and Fermi-LAT Detection of Extended Emission from the Unidentified Source 2HWC J2006+341. *The Astrophysical Journal*, *903*(1), L14. https://doi.org/10.3847/2041-8213/abbfae

Bamba, A., & Williams, B. (2022, November 4). *Supernova remnants: Types and evolution*. https://www.semanticscholar.org/paper/Supernova-remnants%3A-Types-and-evolution-Bamba-Williams/7d61ce2bf6377d2a6465d091cdb03a69e1687d90

Bose, D., & Chitnis, V. R. (2022). Very-high-energy gamma-ray astronomy. *The European Physical Journal Special Topics*, *231*(1), 1–2. https://doi.org/10.1140/epjs/s11734-022-00444-6

Breuhaus, M., Reville, B., & Hinton, J. A. (2022). A pulsar wind nebula origin of the LHAASO-detected UHE gamma-ray sources. *Astronomy & Astrophysics*, *660*, A8. https://doi.org/10.1051/0004-6361/202142097

Catanese, M., & Weekes, T. C. (1999). Very High Energy Gamma-Ray Astronomy. *Publications of the Astronomical Society of the Pacific*, *111*(764), 1193–1222. https://doi.org/10.1086/316435

collaboration, T. F.-L., Ackermann, M., Ajello, M., Allafort, A., Baldini, L., Ballet, J., Barbiellini, G., Baring, M. G., Bastieri, D., Bechtol, K., Bellazzini, R., Blandford, R. D., Bloom, E. D., Bonamente, E., Borgland, A. W., Bottacini, E., Brandt, T. J., Bregeon, J., Brigida, M., … Zimmer, S. (2013). Detection of the Characteristic Pion-Decay Signature in Supernova Remnants. *Science*, *339*(6121), 807–811. https://doi.org/10.1126/science.1231160

Cosmic Rays—Richard Mewaldt. (2009, August 30). https://web.archive.org/web/20090830191145/http://www.srl.caltech.edu/personnel/dick/cos_encyc.html

Fleischhack, H., Burgess, J. M., & Lalla, N. D. (n.d.). *The Multi-Mission Maximum Likelihood Framework threeML: Multi-wavelength astronomy in practice*.

Funk, S. (2015). Ground- and Space-Based Gamma-Ray Astronomy. *Annual Review of Nuclear and Particle Science*, *65*, 245–277. https://doi.org/10.1146/annurev-nucl-102014-022036

Gamma Hadron Separation. (n.d.). Retrieved February 1, 2023, from https://docs.google.com/presentation/d/10i8Wu7HsrZ5HPvKBq-0ATazg21uXOtMKD-n9i9XYkwA

Grenier, I. A., & Harding, A. K. (2015). Gamma-ray pulsars: A gold mine. *Comptes Rendus Physique*, *16*(6), 641–660. https://doi.org/10.1016/j.crhy.2015.08.013

Li, T.-P., & Ma, Y.-Q. (1983). Analysis methods for results in gamma-ray astronomy. *The Astrophysical Journal*, *272*, 317–324. https://doi.org/10.1086/161295

Lyne, A., & Graham-Smith, F. (Eds.). (2012). 8 The Galactic population of pulsars. In *Pulsar Astronomy* (4th ed., pp. 105–116). Cambridge University Press. https://doi.org/10.1017/CBO9780511844584.009

Malone, K. (2018). *A survey of the highest-energy astrophysical sources with the HAWC observatory*. The Pennsylvania State University.

Manchester, R. N., Hobbs, G. B., Teoh, A., & Hobbs, M. (2005). The ATNF Pulsar Catalogue. *The Astronomical Journal*, *129*(4), 1993–2006. https://doi.org/10.1086/428488

Resconi, E., Engel, R., & Gaisser, T. K. (Eds.). (2016a). Acceleration. In *Cosmic Rays and Particle Physics* (2nd ed., pp. 236–257). Cambridge University Press. https://doi.org/10.1017/CBO9781139192194.014

Resconi, E., Engel, R., & Gaisser, T. K. (Eds.). (2016b). Cosmic rays. In *Cosmic Rays and Particle Physics* (2nd ed., pp. 1–11). Cambridge University Press. https://doi.org/10.1017/CBO9781139192194.003

Tepe, A., & Collaboration, the H. (2012). HAWC – The High Altitude Water Cherenkov Detector. *Journal of Physics: Conference Series*, *375*(5), 052026. https://doi.org/10.1088/1742-6596/375/1/052026

VITA
Kenya Mitchell

Education:

Bachelor of Science Degree in Mathematical Sciences, Penn State University, Spring 2024

Minor in Computer Science

Honors in Mathematical Sciences

Thesis Title: Search for New Sources of Very-High-Energy Gamma Rays

Thesis Supervisor: Dr. Miguel Mostafá

Faculty Reader: Dr. Stephane Coutu

Experience:

Honors Service Learning at Bridge of Faith International Ministries, Fall 2023

Supervisor: Mrs. Shelly Best

Internship with Deloitte Consulting LLP, Summer 2023

Undergraduate Research Assistant, September 2021 – Spring 2024

Supervisor: Dr. Miguel Mostafá

Awards:

Dean's List

Outstanding Student in Mathematical Sciences

Activities/Presentations:

Presenter, Poster titled "Search for New Sources of Very-High-Energy Gamma Rays", 2024 Penn State Harrisburg Research Exhibition

Presenter, Poster titled "Search for New Sources of Very-High-Energy Gamma Rays", 2024 Penn State Undergraduate Exhibition,

President, Math Club, Fall 2022 – Fall 2023

Presenter, Poster titled "Observations of TeV Gamma-Ray Pulsars with the High Altitude Water Cherenkov (HAWC) Observatory, 2022 Physics and Nanoscale Materials REU, Penn State University

Presenter, Poster titled "Analzying Orphan TeV Excesses in the 3HWC Catalog", 2022 April APS Meeting, New York City, New York

Grants:

Undergraduate Research Support, Eberly College of Science, 2021 – 2022

Research grant from NASA Pennsylvania Space-Grant Consortium, 2021